ResearchGate

See discussions, stats, and author profiles for this publication at: https://www.researchgate.net/publication/229167969

Direct ab initio dynamics study of the reaction of C2(A3Πu) radical with C2H6

ARTICLE *in* CHEMICAL PHYSICS LETTERS · FEBRUARY 2011

Impact Factor: 1.9 · DOI: 10.1016/j.cplett.2011.01.029

CITATIONS
7

READS
32

6 AUTHORS, INCLUDING:

Jilai Li
Jilin University
66 PUBLICATIONS **287** CITATIONS
SEE PROFILE

Xiang Zhang
Shanxi Teachers University
21 PUBLICATIONS **194** CITATIONS
SEE PROFILE

Dan Mu
Jilin University
166 PUBLICATIONS **1,135** CITATIONS
SEE PROFILE

Available from: Jilai Li
Retrieved on: 25 January 2016

Chemical Physics Letters 503 (2011) 210–214

Contents lists available at ScienceDirect

Chemical Physics Letters

journal homepage: www.elsevier.com/locate/cplett

Direct *ab initio* dynamics study of the reaction of $C_2(A^3\Pi_u)$ radical with C_2H_6

Na Li [a], Rui-Ping Huo [a], Xiang Zhang [b], Xu-Ri Huang [a], Ji-Lai Li [a,*], Chia-Chung Sun [a]

[a] State Key Lab of Theoretical and Computational Chemistry, Institute of Theoretical Chemistry, Jilin University, Changchun 130023, People's Republic of China
[b] School of Chemistry and Materials Science, Shanxi Normal University, Linfen 041004, People's Republic of China

ARTICLE INFO

Article history:
Received 6 November 2010
In final form 12 January 2011
Available online 15 January 2011

ABSTRACT

The reaction of C_2 ($A^3\Pi_u$) with C_2H_6 has been investigated at the BMC–CCSD//BB1K/6-311+G(2d, 2p) level. The classical barrier height for H-abstraction reaction is calculated to be 3.32 kcal/mol and the electron transfer behavior is also analyzed in detail. The rate constants are calculated by TST, CVT, and CVT/SCT over a wide temperature range 50–3000 K. The results indicate: (1) variational effect is small and nonclassical reflection effect is important to the H abstraction in high temperature region; and (2) variational effect is negligible and tunneling effect cooperating with the nonclassical reflection effect makes the rate constant temperature independence in low-temperature range. The CVT/SCT rate constants are in excellent agreement with experimental values.

© 2011 Elsevier B.V. All rights reserved.

1. Introduction

The gas phase kinetics of reactions of the dicarbon C_2 radical with a series of compounds have received increased attention recently due to its considerable importance in air pollution, astrophysics, combustion, and atmospheric chemistry. In addition, being one of the simplest diatomic molecules, the reactions of C_2 with small molecules could provide particularly useful knowledge for the detailed study of the elementary processes in the gaseous phase. C_2 has two low-lying electronic states, the single state $X^1\Sigma_g^+$ and the metastable triplet state $A^3\Pi_u$ (henceforth referred to as $^1C_2$ and $^3C_2$), being separated by only 610 cm^{-1} [1]. $^1C_2$ and $^3C_2$ can be observed directly via laser-induced fluorescence (LIF) using the Swan bands and the Phillips bands of C_2 [2]. Its electronic and structural properties and reactivities have been of a subject of current interests and debates experimentally and theoretically [1,3–24]. However, it is still a long way to have complete understanding of the complexity of this molecule.

Up to now, a large number of experimental and theoretical investigations have been reported on the kinetic information, such as rate coefficients, of $^3C_2$ and $^1C_2$ reactions with a number of hydrocarbons including CH_4, C_2H_2, C_2H_4, C_3H_6, C_3H_8, and so on [3,5,6,8–10,13,16,17,19–24]. Sims and co-workers performed gas-phase experimental studies on the rate coefficients over the low temperature range 24–300 K for the reactions of $^3C_2$ with various hydrocarbons in 2008 [20]. They proposed that the reactivity of the reaction $^3C_2 + C_2H_6$ is very dependent on the nature of the molecule and more specifically, the number of π-bonds which indicates the electrophilic character of the triplet state. Chen [16,21] and Pitts [5,7–9] studied the reactions of $^3C_2$ with a selected series of saturated alkanes (CH_4, C_2H_6, C_3H_8, *n*-C_4H_{10}, *i*-C_4H_{10}, and *n*-C_6H_{14}) by using of pulsed laser photolysis/LIF technique in order to elucidate the reaction mechanisms and the temperature dependence of reactivity. They reported the bimolecular rate constants for these reactions between 298 K and 673 K and provided support for the typical hydrogen abstraction mechanism.

Compared with the reactivity of the triplet state, previous experimental kinetic studies demonstrated that the reactions of $^1C_2$ with hydrocarbons are to be significantly rapid even in very low temperature range 24–300 K and the rate coefficients are typically one order of magnitude higher than that of $^3C_2$ with the exception of CH_4 for saturated hydrocarbons [6,7,9,22]. In addition, a recent study showed that the reactions of $^1C_2$ with unsaturated hydrocarbons are essentially temperature independent in low temperature range 77–296 K, whereas the rate coefficients for the $^3C_2$ reactions are increased until they are equivalent to that of $^1C_2$ at 77 K [19]. Alternatively, positive or negative temperature dependence effects of the rate constants over a certain temperature range for different hydrocarbons, C_2H_6, C_3H_8, *n*-C_4H_{10}, and *i*-C_4H_{10}, etc., for instance, were also found but the tendencies versus the whole temperature range remain unclear [20,21].

Among these reactions, the dynamics behavior and reactivity of reaction of $^3C_2$ ($A^3\Pi_u$) with saturated hydrocarbon C_2H_6 attracts our attention. To our knowledge, the relevant data available in a wide temperature regime remains incomplete and there is no available theoretical study of this reaction despite of its importance. We therefore performed an *ab initio* direct dynamics study on the title reaction $^3C_2 + C_2H_6 \rightarrow {}^{\cdot}C_2H + {}^{\cdot}C_2H_5$. Our aims are to investigate the reaction mechanisms, to obtain 'accurate' theoretical rate constants and to explore to what extent can the theoretical

* Corresponding author.
E-mail addresses: xiangzh2000@hotmail.com (X. Zhang), tcclab@gmail.com (J.-L. Li).

0009-2614/$ - see front matter © 2011 Elsevier B.V. All rights reserved.
doi:10.1016/j.cplett.2011.01.029

predictions be compared with the available experimental results [8,20,21] over the temperature region 24–300 K and 298–673 K, respectively. The temperature dependence of the rate constants is provided over a wide temperature region of 50–3000 K for future study.

2. Computational methods

The equilibrium geometries and harmonic vibrational frequencies of the stationary points involved in the title reaction are calculated using density functional theory (DFT) at the BB1K/6-311+G(2d, 2p) [6-311+G(2d, 2p), B1] level of theory [25]. The minimum energy pathway (MEP) is obtained by intrinsic reaction coordinate (IRC) theory with a gradient step-size of 0.05 $(amu)^{1/2}$ bohr. Then, the first and second energy derivatives are obtained to calculate the curvature of the reaction path and the generalized vibrational frequencies along the reaction path. To obtain more accurate energies and barrier heights, the single point energies (SPE) are refined at the coupled-cluster (CC) theory [26] with single, double, and perturbative treatment of triple excitations CCSD(T) level [27] with B1, 6-311++G(3df, 2pd) [6-311++G(3df, 2pd), B2], and aug-cc-pVTZ [aug-cc-pVTZ, B3] basis sets and at the combined BMC–CCSD method [28] as proposed by Truhlar and co-workers, respectively. It should be noted here that we also performed geometric optimization at the CCSD/6-311G(d, p) and CCSD/6-311+G(2d, 2p) levels to verify the BB1K structural parameters. All the electronic structure calculations are performed by Gaussian 03 program package [29].

The theoretical rate constants are calculated with the Polyrate 9.7 program package [30]. The rate constants are calculated using the conventional transition state theory (TST) [31], canonical variational transition state theory (CVT) [32,33], and canonical variational transition state incorporating a small-curvature tunneling correction(CVT/SCT) method [31]. The Euler single-step integrator with a step size of 0.0001$(amu)^{1/2}$ bohr is used to follow the MEP. The curvature components are calculated using a quadratic fit to obtain the derivative of the gradient with respect to the reaction coordinate. Within the temperature range 50–3000 K, the rate constants at selected temperature points are calculated using mass-scaled Cartesian coordinate.

Quasi-restricted molecular orbital (QRO) [34] of special points along the MEP are calculated by Orca 2.8 program package [35] and plotted using Chimera [36].

3. Results and discussion

3.1. Stationary points and reaction mechanism

The geometric parameters of the reactants, products and transition state of the title reaction are optimized at the BB1K/6-311+G(2d, 2p), CCSD/6-311G(d, p) and CCSD/6-311+G(2d, 2p) levels as shown in Figure 1. The coordinates and harmonic frequencies of the reactants, products and transition states, and available experimental values are listed in Supporting Materials Tables S1 and S2.

In Figure 1, selected bond lengths and bond angles are given. The geometry parameters of all species calculated by both BB1K and CCSD methods are in good agreement with available experimental data. In the transition structure TS, the C–H bond of C_2H_6 is stretched by 14% over its equilibrium structure in C_2H_6 and the C–H bond going to be formed is about 31% longer than that in the product C_2H. The bond lengths being formed (C–H in C_2H) and broken (C–H in C_2H_6) at the saddle point are in the ranges 1.39–1.06 and 1.09–1.23 Å, respectively. Hence, the less stretch of the breaking bond than that of the forming bond indicates a reactant-like transition state TS, i.e., the H-abstraction channel process is via an early transition state. The harmonic vibrational frequencies of all the reactants, TS and products at the BB1K/6-311+G(2d, 2p) level are also in good agreement with available experimental results [37–39]. The TS possesses one and only one imaginary frequency *i*484 cm^{-1}, indicating that the transition state is a real first-order saddle point.

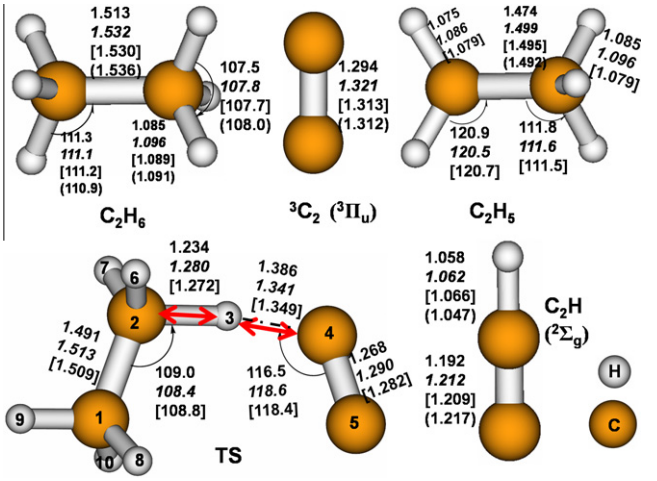

Figure 1. Geometric parameters of various species involved in the title reaction. Bond length in angstrom and angle in degree. The normal, italics, square brackets and in parentheses are at the BB1K/6-311+G(2d, 2p), UCCSD/6-311G(d, p), UCCSD/6-311+G(2d, 2p) levels, and experimental data, respectively. The red arrows show the harmonic vibrational mode in the transition state. Experimental data: C_2H_6, Ref. [41]; $^3C_2$, Ref. [42]; C_2H, Ref. [41]. (For interpretation of the references to color in this figure legend, the reader is referred to the web version of this article.)

The detailed electron transfer analysis is carried out along the minimal energy pathway by quasi-restricted molecular orbital calculations with Orca program. Figure 2 shows the schematic molecular orbital diagrams for the reactants, transition states and products involved in the reaction of $^3C_2 + C_2H_6$. By analysis of the corresponding molecular orbital, we can draw the conclusion that during the H-atom abstraction process, one β electron in C–H bond of C_2H_6 is shifted to the π_{2p}-orbital of $^3C_2$, leading to the ethyl radical with one α electron left. Figure 3 describes the spin density changes upon the reaction process. As the reaction going on, the spin density of 2C increased concomitantly with that decreased in 4C. Moreover, the spin densities of ^{1}C, 3H and 5C are nearly unchanged. These spin density results confirm our electronic analysis mentioned above (Figure S1). To sum up, the overall mechanism of the title reaction is better described as following: as C_2H_6 and $^3C_2$ gradually approaches with each other, one of H-atoms in C_2H_6 is abstracted by one C atoms in $^3C_2$, leading to two radicals $\cdot C_2H$ and $\cdot C_2H_5$ generated.

3.2. Energetics

In order to construct a reliable MEP for the rate constant calculations, we refined the SPE of stationary points by CCSD(T) method with basis sets B1, B2 and B3, and the combined method BMC–CCSD, respectively. The electronic structure energies, zero-point correction energies and relative energies of all stationary points at various levels of theory are listed in Tables S3–S6.

The schematic PESs of the title reaction constructed at the CCSD(T)/B1, CCSD(T)/B2, CCSD(T)/B3 and BMC–CCSD levels are given in Figure 4. The total energy of the reactants $^3C_2 + C_2H_6$ is set at zero as a reference for other species involved in the title reaction. As shown in Figure 4, the BMC–CCSD gives the lowest energy barrier 0.4 kcal/mol among the four levels of theory, and the CCSD(T) energy barrier heights ΔE decrease (2.8 → 1.7 → 1.3 kcal/mol) with increasing basis set size B1 → B2 → B3. This tendency suggests

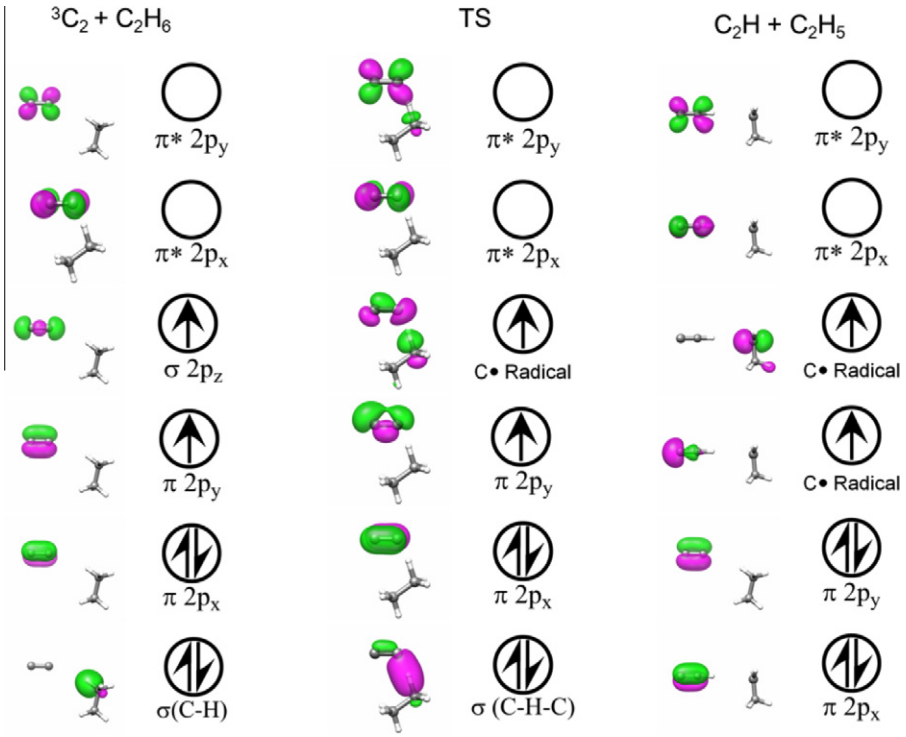

Figure 2. Schematic MO diagrams of reactants ($^3C_2 + C_2H_6$), transition state (TS) and products ($C_2H + C_2H_5$).

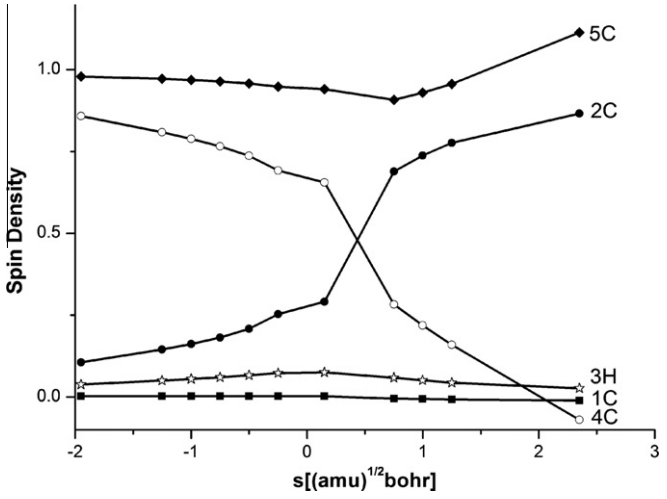

Figure 3. The change of atomic spin densities on 1C, 2C, 3H, 4C and 5C obtained from selected points on IRC pathway obtained with ORCA program.

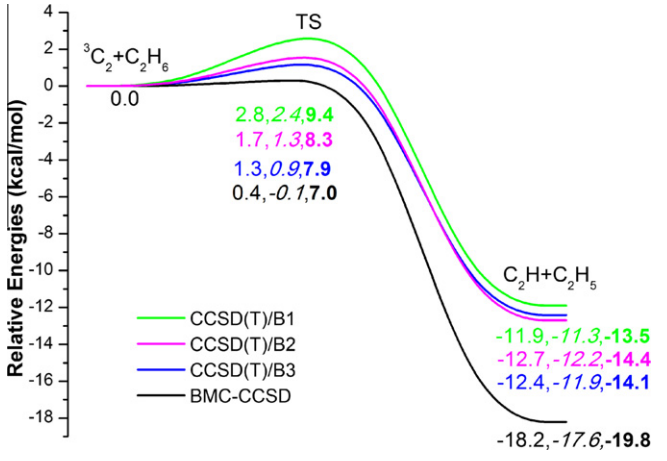

Figure 4. Potential energy profiles for the reaction of $^3C_2 + C_2H_6 \rightarrow C_2H + C_2H_5$ in units of kcal/mol with ZPE correction. Green line, CCSD(T)/B1//BB1K/B1; magenta line, CCSD(T)/B2//BB1K/B1; blue line, CCSD(T)/B3//BB1K/B1; black line, BMC–CCSD//BB1K/B1. The normal, italics, and bold values are ΔE, ΔH and ΔG, respectively. (For interpretation of the references to color in this figure legend, the reader is referred to the web version of this article.)

that, given larger basis sets used, the CCSD(*T*) barrier height is very likely to become close to that of BMC–CCSD. The barrier height of BMC–CCSD method which seems to be more reliable is also in accordance with Truhlar's prediction, that is, besides many thermodynamic properties, BMC–CCSD method is optimized specially against many reactions for barrier height [28]. Furthermore, the reaction is exothermic ΔH −17.6 kcal/mol at the BMC–CCSD level at 298 K, which is in good agreement with the experimental predictions [8,16]. Considering the efficiency and precision, it is therefore safe to make the conclusion that the combination of the BMC–CCSD//BB1K methods can provide satisfied results for analogous systems. So, we refined the SPE of selected points on the BB1K MEP using the BMC–CCSD method for the following rate constant calculations.

3.3. Rate constants

The rate constants of the title reaction are calculated over a wide temperature range of 50–3000 K using the TST, CVT, and CVT/SCT methods. A total 20 points near the transition state, 10 on reactants side and 10 on product side, are selected to obtain the potential surface information along the MEP. The calculated TST, CVT and CVT/SCT rate constants at the BMC–CCSD//BB1 K level are listed in Table S7, in which the available experimental rate constants in the temperature range 298–673 K are also given.

Figure 5 presents the plot of the classical potential energy curve $V_{MEP(s)}$, the vibrationally adiabatic ground-state potential curve

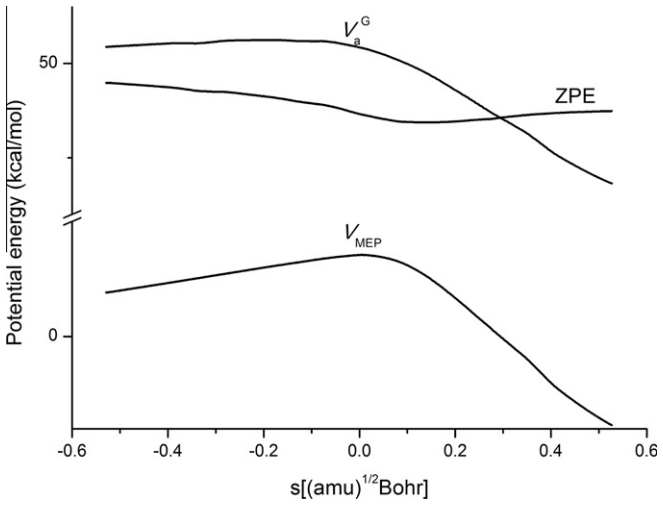

Figure 5. Classical potential energy curve (V_{MEP}), ground-state vibrationally adiabatic curve (V_a^G), and ZPE curve as functions of s [(amu)$^{1/2}$bohr] at the BMC–CCSD//BB1K/B1 level for the title reaction.

$V_a^G(s)$, and the zero-point energy (ZPE) as functions of the intrinsic reaction coordinate s (amu)$^{1/2}$ bohr at the BMC–CCSD//BB1K level, where $V_a^G = V_{MEP} + ZPE$. As shown in Figure 5, the V_a^G and V_{MEP} curves are similar in shape, implying variational effect is less important. The ZPE curve is practically constant as s varies, with only a gentle drop near the saddle point $s = 0$. This drop offers a good explanation of the lower effective barrier height 0.35 kcal/mol than the classical one 3.32 kcal/mol and the more flat of V_a^G curve, implying that quantum effect (including tunneling and nonclassical reflection) will be large for the rate constant calculation. The following study of rate constants will further testify this view point.

The BMC–CCSD//BB1K/B1 rate constants in the temperature range 50–3000 K and experimental values are plotted as functions of the reciprocal of temperature in Figure 6. As shown in Figure 6, the CVT rate constants are slightly smaller than those of TST when $T > 200$ K, while the rate constants for CVT and TST are almost the same when $T < 200$ K. This indicates that the variational effect for the reaction is small in high temperature range and is negligible in low temperature region. As for the CVT/SCT and CVT rate constants, the big discrepancy between them implies the importance of the small-curvature tunneling correction and hence it should be considered in the title reaction. The CVT/SCT rate constant is smaller than that of CVT in the $T > 100$ K range. This may be well rationalized by the quantum effect as pointed out by Parsafar [40]. The quantum effect here comes mainly from the nonclassical reflection effect which precludes particles to pass over the classical barrier. And the title reaction can be referred as a special case in which the reaction is reflected back to reactant side at energies above the barrier due to the nonclassical reflection effect. The nonclassical reflection effect is very important to the hydrogen abstraction and decreases the CVT/SCT rate constants. In the $T < 100$ K range, the CVT/SCT rate constant becomes a constant and it is larger than that of CVT, indicating the counteractions of the tunneling effect against the nonclassical reflection effect. It appears that the CVT/SCT rate constant is in good agreement with available experimental data given by Hu et al. [16,21] and Pasternack et al. [8]. The normal Arrhenius expression of $k(T) = 2.6996 \times 10^{-11}\exp(-(1034.17 \pm 51.57)/T)$ cm^3 molecule^{-1} s^{-1} fits of the CVT/SCT rate constants between 298 K and 673 K. Consequently, the calculated activation energy $E_a = 2.14$ kcal/mol is very close to the experimental value 1.83 ± 0.03 kcal/mol [8,21].

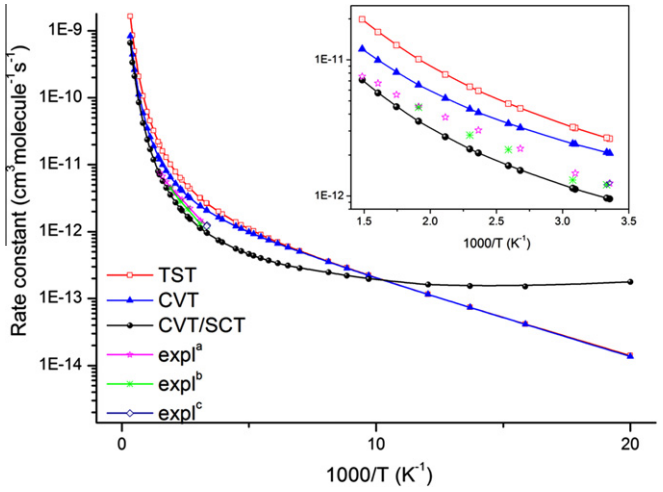

Figure 6. Plot of the TST, CVT, and CVT/SCT rate constants calculated at the BMC–CCSD//BB1K/B1 level versus 1000/T between 50 K and 3000 K for the title reaction. Red line, TST; blue, CVT; black, CVT/SCT. For clarity, the experimental temperature region between 298 and 673 K is amplified and given in the inset. Expl^a, Ref. [21]; Expl^b, Ref. [8]; Expl^c, Ref. [16]. (For interpretation of the references to color in this figure legend, the reader is referred to the web version of this article.)

In order to facilitate the future experimental measurements, the normal (k^2) and three-parameter (k^3) Arrhenius equations fitting of the CVT/SCT rate constants and the activation energies of the title reaction in three temperature ranges from 100 K to 3000 K are performed and the expressions are given as follows: (in unit of cm^3 molecule^{-1} s^{-1}).

$k^2_{(100-300)} = 1.65 \times 10^{-12}\exp(-234.1/T)$ $E_a = 0.49$ kcal/mol
$[100 \leqslant T \leqslant 300$ K]
$k^2_{(300-1000)}$ $5.54 \times 10^{-11}\exp(-1315.8/T)$ $E_a = 2.72$ kcal/mol
$[300 \leqslant T \leqslant 1000$ K]
$k^2_{(1000-3000)} = 2.72 \times 10^{-9}\exp(-4925.6/T)$ $E_a = 9.93$ kcal/mol
$[1000 \leqslant T \leqslant 3000$ K]
$k^3_{(100-300)} = 4.5214 \times 10^{-19}(T)^{2.45689}\exp(-165.0/T)$
$[100 \leqslant T \leqslant 300$ K]
$k^3_{(300-1000)} = 1.6315 \times 10^{-12}(T)^{3.64543}\exp(-513.8/T)$
$[300 \leqslant T \leqslant 1000$ K]
$k^3_{(1000-3000)} = 8.5140 \times 10^{-19}(T)^{2.58608}\exp(734.5/T)$
$[1000 \leqslant T \leqslant 3000$ K]

4. Conclusion

In this Letter, we employed direct *ab initio* dynamics method to study the title reaction $^3C_2 + C_2H_6 \rightarrow {}^{\cdot}C_2H + {}^{\cdot}C_2H_5$. Based on the IRC pathway, the electron transfer behavior is analyzed by quasi-restricted orbital method in detail. Electronic structure analysis indicates that it occurs via H-abstraction mechanism conclusively. The rate constants are calculated over a wide temperature range of 50–3000 K, using the TST, CVT, CVT/SCT methods at the BMC–CCSD//BB1K/6-311+G(2d, 2p) level of theory. The results demonstrate that the variational effect is small in high temperature range and is negligible in low temperature region. However, quantum effect plays an important role in rate constant calculations of the H-abstraction: the nonclassical reflection is predominant when $T > 200$ K, while the tunneling effect is predominant in low temperature region $T < 100$ K. The CVT/SCT rate constants are in good agreement with available experimental data and the normal Arrhenius expression is $k(T) = 2.6996 \times 10^{-11}\exp(-1034.17/T)$ cm^3 molecule^{-1} s^{-1} between 298 K and 673 K. The normal and three-parameter expressions of Arrhenius rate constants are also provided within 100–3000 K. Our theoretical study is expected to gain further insight into the reaction dynamics behavior over a

wide temperature range, in particular, the range where no experimental data are available so far.

Acknowledgments

This work is supported by the National Natural Science Foundation of China (NSFC No. 21073075), Research Fund for the Doctoral Program of Higher Education of China (RFDP No. 20100061 110046), the Special Funding of State Key Laboratory of Theoretical and Computational Chemistry, Jilin University and Basic Research Fund of Jilin University (No. 421010061439). The authors are thankful for the reviewers' invaluable comments.

Appendix A. Supplementary data

Supplementary data associated with this article can be found, in the online version, at doi:10.1016/j.cplett.2011.01.029.

References

[1] E.A. Ballik, D.A.J. Ramsay, Chem. Phys. 31 (1959) 1.
[2] G. Herzberg, Spectra of Diatomic Molecules, Van Nostrand, Princeton, New Jersey, 1950.
[3] H. Reisler, M. Mangir, C. Wittig, J. Chem. Phys. 71 (1979) 2109.
[4] M.S. Mangir, H. Reisler, C. Wittig, J. Chem. Phys. 73 (1980) 829.
[5] L. Pasternack, A.P. Baronavski, J.R. McDonald, J. Chem. Phys. 73 (1980) 3508.
[6] H. Reisler, M. Mangir, C. Wittig, Chem. Phys. 47 (1980) 49.
[7] H. Reisler, M.S. Mangir, C. Wittig, J. Chem. Phys. 73 (1980) 2280.
[8] L. Pasternack, W.M. Pitts, J.R. McDonald, Chem. Phys. 57 (1981) 19.
[9] W.M. Pitts, L. Pasternack, J.R. McDonald, Chem. Phys. 68 (1982) 417.
[10] P.S. Skell, L.M. Jackman, S. Ahmed, M.L. McKee, P.B. Shevlin, J. Am. Chem. Soc. 111 (1989) 4422.
[11] M. Gong, Y. Bao, R.S. Urdahl, W.M. Jackson, Chem. Phys. Lett. 217 (1994) 210.
[12] S.A. Maluendes, A.D. McLean, E. Herbst, Chem. Phys. Lett. 217 (1994) 571.
[13] D.A. Horner, L.A. Curtiss, D.M. Gruen, Chem. Phys. Lett. 233 (1995) 243.
[14] V.M. Blunt, H. Lin, O. Sorkhabi, W.M. Jackson, Chem. Phys. Lett. 257 (1996) 347.
[15] C. Huang, D. Zhao, L. Pei, C. Chen, Y. Chen, Chem. Phys. Lett. 389 (2004) 230.
[16] C. Huang, Z. Zhu, Y. Xin, L. Pei, C. Chen, Y. Chen, J. Chem. Phys. 120 (2004) 2225.
[17] A.M. Mebel, V.V. Kislov, R.I. Kaiser, J. Phys. Chem. A 110 (2006) 2421.
[18] A. Paramo, A. Canosa, S.D. Le Picard, I.R. Sims, J. Phys. Chem. A 110 (2006) 3121.
[19] N. Daugey, P. Caubet, A. Bergeat, M. Costes, K.M. Hickson, Phys. Chem. Chem. Phys. 10 (2008) 729.
[20] A. Paramo, A. Canosa, S.D. Le Picard, I.R. Sims, J. Phys. Chem. A 112 (2008) 9591.
[21] R. Hu, Q. Zhang, Y. Chen, J. Chem. Phys. 132 (2010) 164312.
[22] A. Canosa, A. Paramo, S.D. Le Picard, I.R. Sims, Icarus 187 (2007) 558.
[23] V.M. Donnelly, L. Pasternack, Chem. Phys. 39 (1979) 427.
[24] L. Pasternack, J.R. McDonald, Chem. Phys. 43 (1979) 173.
[25] Y. Zhao, B.J. Lynch, D.G. Truhlar, J. Phys. Chem. A 108 (2004) 2715.
[26] G.E. Scuseria, H.F. Schaefer, J. Chem. Phys. 90 (1989) 4.
[27] J.A. Pople, M.H. Gordon, K. Raghavachari, J. Chem. Phys. 87 (1989) 8.
[28] B.J. Lynch, Y. Zhao, D.G. Truhlar, J. Phys. Chem. A 109 (2005) 1643.
[29] M.J. Frisch et al., Gaussian 03, Revision D.02, Gaussian, Inc., Wallingford, CT, 2004, 2006.
[30] C. José et al., Version 9.7, Department of Chemistry and Supercomputing Institute, University of Minnesota, Minneapolis, Minnesota 55 455, 2007.
[31] Y.P. Liu, G.C. Lynch, T.N. Truong, D.H. Lu, D.G. Truhlar, B.C. Garrett, J. Am. Chem. Soc. 115 (1993) 2408.
[32] B.C. Garrett, D.G. Truhlar, J. Chem. Phys. 70 (1979) 1593.
[33] B.C. Garrett, D.G. Truhlar, J. Am. Chem. Soc. 101 (1979) 4534.
[34] F. Neese, J. Am. Chem. Soc. 128 (2006) 10213.
[35] F. Neese, Orca – an *ab initio*, Density Functional and Semiempirical Program Package, Version 2.8, Bonn University, 2010.
[36] E.F. Pettersen, T.D. Goddard, C.C. Huang, G.S. Couch, D.M. Greenblatt, E.C. Meng, T.E. Ferrin, J. Comput. Chem. 25 (2004) 1605.
[37] J.W. Stephens, W.-B. Yan, M.L. Richnow, H. Solka, R.R. Curl, J. Mol. Struct. 190 (1988) 41.
[38] H. Kanamori, E. Hirota, J. Chem. Phys. 89 (1988) 8.
[39] M. Bogey, C. Demuynck, J.L. Destombes, Mol. Phys. 66 (1989) 955.
[40] M. Taghikhani, G.A. Parsafar, H. Sabzyan, J. Phys. Chem. A 109 (2005) 8158.
[41] K.E. Kuchitsu, Structure of Free Polyatomic Molecules – Basic Data, Springer, Berlin, 1998.
[42] H.B. Gray, Chemical Bonds, Benjamin, Menlo Park, CA, 1973.